

4

2020

2021

Muon Phase-2 Upgrade

2022 In Chapter 2, the timeline of the LHC has been described and the upcoming High Luminosity LHC
2023 was introduced. LS3 has now started and the first HL-LHC related upgrade of CMS will take place.
2024 In order to understand the context in which the work of this thesis was performed as well as its
2025 motivations, it is necessary to give more insight into the reasons behind the increased instantaneous
2026 luminosity of LHC. In a first section of the chapter, these motivations will be discussed.

2027 The muon system of CMS will then be presented in greater details than what was done in Chapter
2028 ?? in order to have a better understanding of the need for upgrades of its different sub-systems in
2029 the perspective of HL-LHC. Most of the detectors will require new electronics to adapt to the new
2030 data flow and be integrated into a more robust trigger. Moreover, the redundancy of the muon system
2031 in the endcaps will need to be improved. This will be achieved by the addition of new detectors.

2032 Finally, some insight will be given on ecofriendly gas studies for the specific case of Resistive
2033 Plate Chambers. These studies don't fall into the scope of the HL-LHC upgrades but the necessity
2034 of operating the detectors with gas mixtures that are more respectful of the environment is real. The
2035 European union is starting to press the scientific community for solutions and the research institutes
2036 are investing time into finding replacements to the gases used while maintaining similar working
2037 performances.

2038 4.1 Motivations for HL-LHC and the upgrade of CMS

2039 As detailed in Section 2.2.2, the first data taking period, during which the LHC was only operated
2040 at a center-of-mass energy of 7 TeV, took place until the start of LS1. It has been sufficient to
2041 claim the discovery of a new $125 \text{ GeV}/c^2$ particle compatible with the Higgs boson by both CMS
2042 and ATLAS in July 2012 and hence achieve a major milestone in the history of science towards the
2043 understanding of the fundamental nature of the universe. Nevertheless, the LHC machine holds the
2044 potential to go further and help unravel the remaining mysteries the High-Energy Physics (HEP)
2045 community is facing.

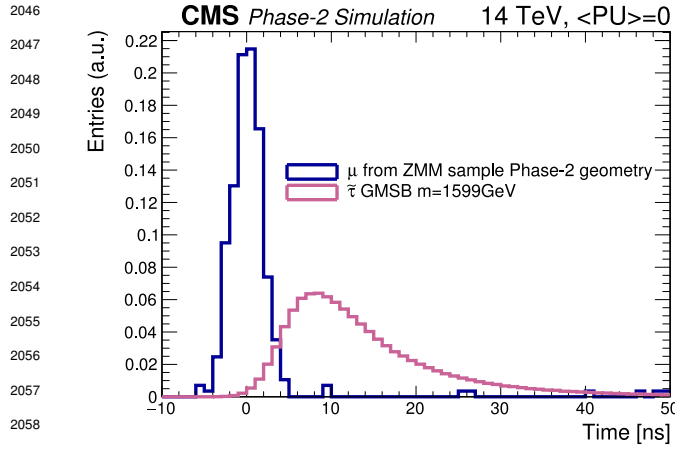


Figure 4.1: The measured transit time of an HSCP in CMS is compared to the transit time of a particle traveling at near the speed of light [177].

heavy gauge boson studies would also see their mass range limits pushed away by at least 1 TeV and could lead to a new breakthrough. Many of the Standard Model extensions discussed in Section 2.1.3 yield Heavy Stable Charged Particles (HSCPs), i.e. heavy long-lived particles. These particles would be produced at the LHC with a high momentum but a velocity significantly lower than the speed of light ($\beta < 0.9$) [238–242] and/or a charge that differs from the elementary charge ($|Q| = e$, $|Q| < e$ or $|Q| > e$) [241–246]. Depending on the model considered, HSCPs could be lepton-like heavy particles or on the contrary R-hadron, i.e. particles composed of a supersymmetric particle and at least one quark [241].

Over its full lifetime, the HL-LHC is expected to deliver an outstanding integrated luminosity of 3000 fb^{-1} , nearly an order of magnitude higher than what will be delivered by LHC until LS3 starts, as shown in Figure 2.20. In the case of Higgs studies, this will lead to measuring the couplings of the boson to a precision of 2 to 5%. Thanks to the estimated 15 millions of Higgs bosons created every year, a more precise measurement of potential deviations from the theoretical predictions is expected. The properties of the boson will hence be tested and compared to the SM Higgs neutral boson.

SUSY and

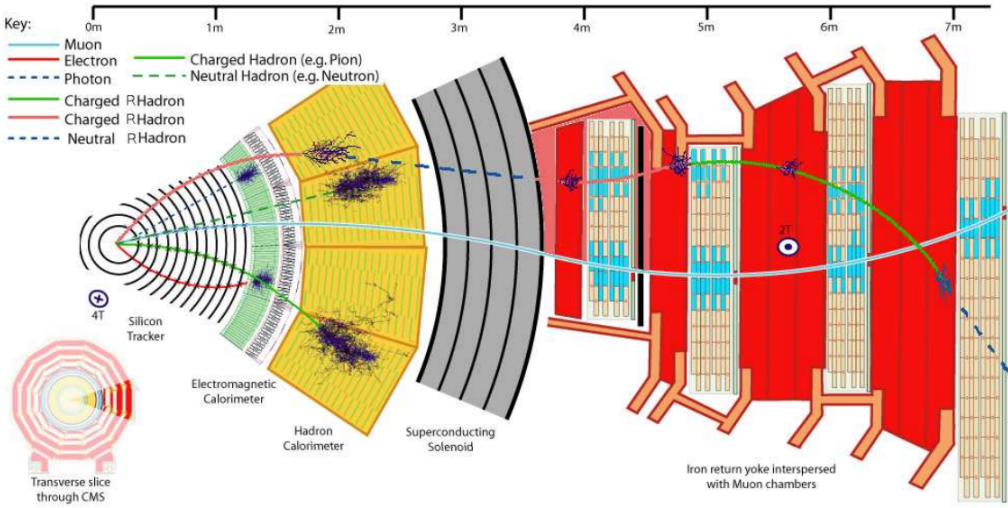


Figure 4.2: Slice of the CMS detector showing examples of passage of SM particles and R-hadrons. On the one hand, lepton-like HSCPs will appear to behave like slow and heavy muons. On the other hand, R-hadrons are likely to convert into other kind of charged or neutral R-hadrons due to interactions inside the detector volume.

2072 Due to lifetimes of the order of a few ns,
 2073 HSCPs would travel for long enough distances
 2074 to cross through entire typical collider detec-
 2075 tors while appearing almost stable. Because
 2076 of their low velocity, they can be reconstructed
 2077 and assigned to bunch crossings different to
 2078 the ones they effectively have been produced,
 2079 as shown in Figure 4.1, if reconstructed at
 2080 all. Indeed, the trigger algorithms in use at
 2081 CMS were not designed for such slow parti-
 2082 cles, and they assume most particles of inter-
 2083 est will have a velocity close to the speed of
 2084 light [242, 247].

2085 As HSCPs are long-lived particles, their
 2086 identification would be possible thanks to the
 2087 muon system. The main background will con-
 2088 sist of wrongly measured muons which should
 2089 have a lower transverse momentum, a near to
 2090 speed-of-light velocity and a low ionisation
 2091 energy loss. An example of passage of HSCPs
 2092 through a slice of the CMS detector is showed
 2093 in Figure 4.2. The tracks associated to the
 2094 HSCPs would then have to be reconstructed in
 2095 both the silicon detectors, for precise dE/dx
 2096 measurement, and the muon system detectors. In this case, the muon system will be used to perform
 2097 Time-of-flight (ToF) measurements to discriminate between near speed-of-light particles and slower
 2098 ones. The full reconstruction will then look for useful signatures such as the large transverse mo-
 2099 mentum of the candidates, or their large ionisation energy loss alongside the low velocity accurately
 2100 measured thanks to the muon system as depicted in Figure 4.3. The ToF measurement to identify
 2101 beyond the Standard Model particles will mostly rely on the time information provided by the Drift
 2102 Tubes, in the barrel region of the detector, and Cathode Strip Chambers, in the endcaps. From CMS
 2103 point of view, it will then become necessary to increase the acceptance and redundancy of the end-
 2104 caps toward higher pseudo-rapidity as the pseudo-rapidity region $1.6 < |\eta| < 2.5$ is only covered
 2105 by CSCs.

2106
 2107 A natural consequence of the higher instantaneous luminosity will be the increase of collisions
 2108 per bunch crossing. It is estimated that the pile-up will rise from the approximate average of 40
 2109 collisions per bunch crossing in 2017 and 2018, presented in Figure 4.4, to 140 to 200 depending on
 2110 the scenario considered [248]. The trigger rate will then be affected in the same way putting a lot
 2111 of stress on the trigger algorithms. Upgrading the electronics of some of the detectors and working
 2112 on the data flow within the experiment would help going through HL-LHC with keeping similar
 2113 performance than during Phase-1. On the other hand, the impact of the increased background will
 2114 become problematic in many ways and will force for upgrades or many sub-systems of CMS. The
 2115 main effects will be a large increase of the irradiation of the detectors, mainly close to the beam
 2116 line. Both the detectors already installed and the new detectors that will extend the coverage of the

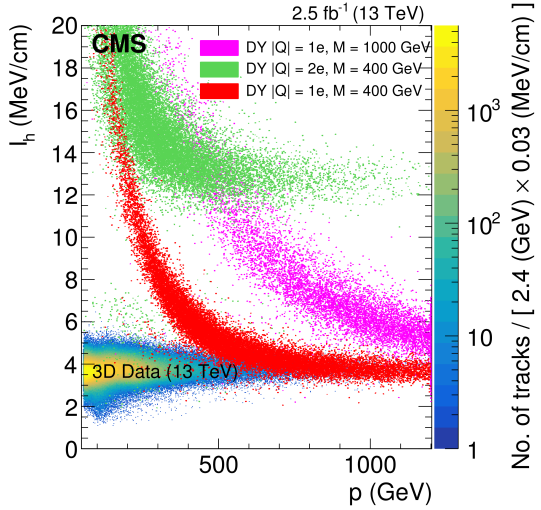


Figure 4.3: Distribution of the energy-loss dE/dx as described by Bethe-Bloch formula through the estimator I_h with increasing particle momentum for tracks in the 13 TeV data. The estimator depends on the charge deposition of the particles per unit length in the silicon detectors of CMS which is related to their energy loss as explained in a publication by the CMS Collaboration [241]. The simulated HSCPs are singly or multiply charged particles with masses of 400 and 1000 GeV.

muon system toward higher pseudo-rapidity need to be certified for the irradiation levels they will be subjected to until the end of HL-LHC. Simulations of the expected distribution of absorbed dose in the CMS detector under HL-LHC conditions show, in Figure 4.5, that detectors placed close to the beam line will have to withstand high irradiation, the radiation dose being of the order of a few tens of Gy.

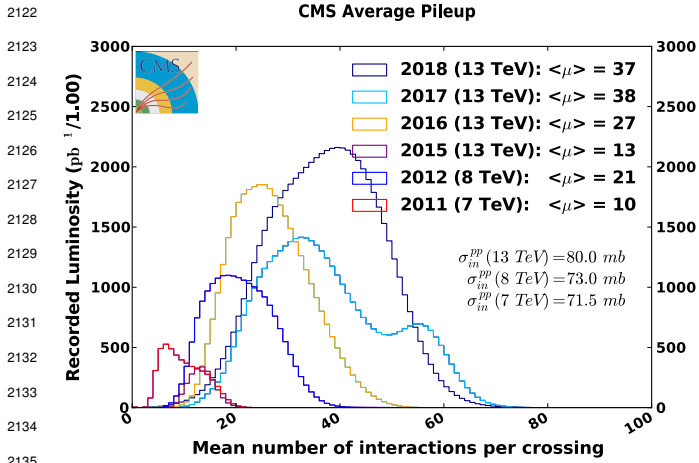


Figure 4.4: Distribution of the average number of interactions per crossing (pileup) for pp-collisions in 2011 (red), 2012 (blue), 2015 (purple), 2016 (orange), 2017 (light blue), and 2018 (navy blue). The overall mean values and the minimum bias cross sections are also shown [249].

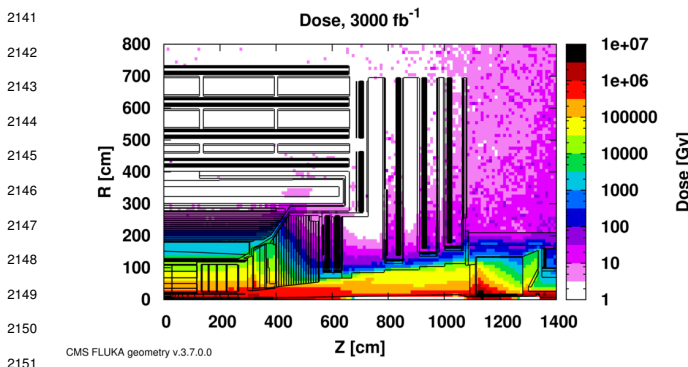


Figure 4.5: Absorbed dose in the CMS Cavern after an integrated luminosity of 3000 fb^{-1} . Using the interaction point as reference, R is the transverse distance from the beamline and Z is the distance along the beamline [177].

4.0 but the identification of muons and measurement of their energy with reasonable precision only using the tracker is nearly impossible. Thus, this increased tracker coverage range needs to be put in parallel with a matching muon detector and will open doors to multi-lepton final states in which leptons are likely to have a low transverse momentum and to be found near the beam line.

Finally, as the muon system is composed only of gaseous detectors, strong environmental concerns have risen over the last years as the European directives will restrict the use of fluorine based gas mixtures. Both the CSC and RPC subsystems, using CF_4 , $C_2H_2F_4$, or SF_6 , will need to adapt

Improving this situation will come with the increase of hit numbers recorded along the particle track to reduce the ambiguity on muon versus background detection. Moreover, the measurement of small production cross-section and/or decay branching ratio processes, such as the Higgs boson coupling to charge leptons, and in particular to muons, or the $B_s \rightarrow \mu^+ \mu^-$ decay, is of major interest. Such considerations give more weight to the upgrade of the forward regions to maximize the physics acceptance to the largest possible solid angle.

To ensure proper trigger performance within the present coverage, the muon system will be completed with new chambers, and the electronics of the present system will need to be upgraded. A first step into this direction will be taken by installing new gaseous detectors in each endcap layer and extend the coverage up to $|\eta| = 2.8$. Nevertheless, the region beyond $|\eta| > 2.8$ and extending to $|\eta| = 5.0$ only is covered by the forward HCAL detectors and lack redundant muon detector coverage. Extensions of the tracker in the context of HL-LHC will increase its coverage up to $|\eta| =$

2163 their working gas in order to strongly reduce the greenhouse potential of the mixtures released into
 2164 the atmosphere due to gas leaks.

2165 4.2 Necessity for improved electronics

2166 Drift Tubes and Cathode Strip
 2167 Chambers are important compo-
 2168 nents used to identify and measure
 2169 muons, especially thanks to their
 2170 spatial resolution of the order of
 2171 $100\text{ }\mu\text{m}$. Nevertheless, the lumi-
 2172 nosity and irradiation during HL-
 2173 LHC will cause serious event loss
 2174 and ageing on the electronics of
 2175 these subsystems that will comprise
 2176 the triggering and data transferring
 2177 needs of CMS. Thus, electronics up-
 2178 grade is foreseen to address these
 2179 expected problems. While only
 2180 the RPCs' electronic system is able
 2181 to operate under Phase-2 require-
 2182 ments [250], DTs and CSCs will
 2183 need to improve their trigger accept-
 2184 ance rate and latency to ensure that the Level-1 trigger thresh-
 2185 old can stay at the same level [251]. The Level-1 trigger consists of custom hardware processors
 2186 receiving data from the calorimeters and the muon system. In return, they generate a trigger signal
 2187 within $3\text{ }\mu\text{s}$, with a maximum rate of 100 kHz. In the perspective of HL-LHC, each subsystem needs
 2188 to achieve a minimum rate of 500 kHz with a latency not greater than $12.5\text{ }\mu\text{s}$. DTs and CSCs will
 2189 also need to improve their Data Acquisition (DAQ) transfer rate to reach a minimum near 1 Tbit/s.
 The foreseen upgrades are expected to exceed the requirements.

2190 The first version of Minicrate
 2191 electronics (MiC1) used by DTs
 2192 don't allow for high enough trig-
 2193 ger rate. In addition to this prob-
 2194 lem, it was shown that these elec-
 2195 tronics contain components that are
 2196 not radiation hard enough to sus-
 2197 tain HL-LHC conditions and hence,
 2198 a too large number of channels may
 2199 fail due to radiations as showed in
 2200 Figure 4.6. The MiC1 will be re-
 2201 placed on each detector by an im-
 2202 proved version referred to as MiC2
 2203 while Front-End Electronics (FEE)
 2204 and High Voltage (HV) modules
 2205 will not need any replacement. On the other hand, CSCs showed that their electronics would be

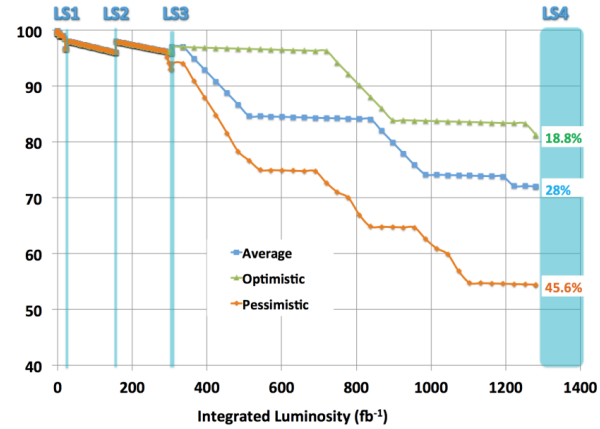


Figure 4.6: Extrapolated fraction of failing channels of the present DT MiC1 electronics as a function of the integrated luminosity for different scenarios until LS4 [177].

2190 The first version of Minicrate
 2191 electronics (MiC1) used by DTs
 2192 don't allow for high enough trig-
 2193 ger rate. In addition to this prob-
 2194 lem, it was shown that these elec-
 2195 tronics contain components that are
 2196 not radiation hard enough to sus-
 2197 tain HL-LHC conditions and hence,
 2198 a too large number of channels may
 2199 fail due to radiations as showed in
 2200 Figure 4.6. The MiC1 will be re-
 2201 placed on each detector by an im-
 2202 proved version referred to as MiC2
 2203 while Front-End Electronics (FEE)
 2204 and High Voltage (HV) modules
 2205 will not need any replacement. On the other hand, CSCs showed that their electronics would be

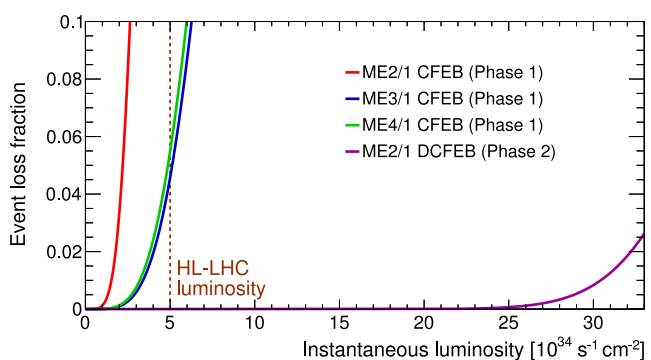


Figure 4.7: The event loss fractions as a function of the instantane-
 ous luminosity is compared for CFEBs (Phase-1) and
 DCFEBs (Phase-2) at different CSC locations. HL-LHC lumino-
 sity is marked with the dashed brown line [177].

able to live through the 10 years of Phase-2, but the limited buffer depth might cause memory overflows and read-out inefficiencies with a fraction of event loss ranging from 5 to more than 10% at an instantaneous luminosity similar to which of HL-LHC depending on the expected background. The replacement of CSCs' CFEBs by digital ones, DCFEBs, with a deeper buffer would permit to make event loss negligible and satisfy HL-LHC requirements as can be seen in Figure 4.7. All these new DT and CSC electronics will be connected to the trigger electronics via optical links to ensure a faster communication [177].

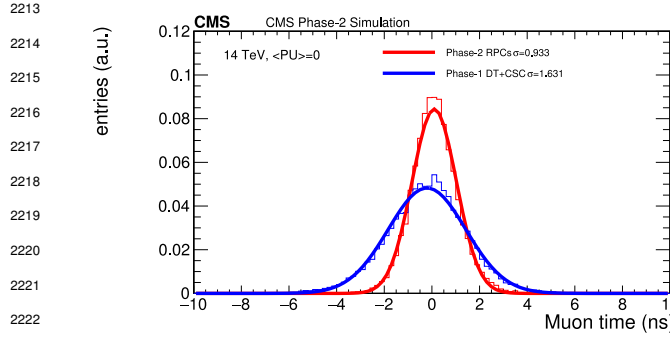


Figure 4.8: Comparison of the simulated time residuals in between reconstructed and true muon times without (blue) and with (red) the upgraded RPC link system [177].

components may become the source of failing channels throughout Phase-2. Moreover, these link boards were originally designed only to match RPC digitized signals with the corresponding bunch crossing. Due to this feature, the time resolution of the full RPC chain is hence limited to 25 ns and does not make use of the full time resolution of the detectors. The time resolution foreseen after the upgrade can be seen through Figure 4.8 and is of the order of 1 ns.

The upgrade on the side of Resistive Plate Chambers will not be done at the level of the electronics but rather that of the Link System located in the service cavern of CMS. RPC Link System connects the front-end electronics data of RPCs into CMS trigger processors. The main motivation for such an upgrade is that the electronic board composing the link system are built using obsolete and/or weak components that can easily suffer from the electromagnetic noise. These components

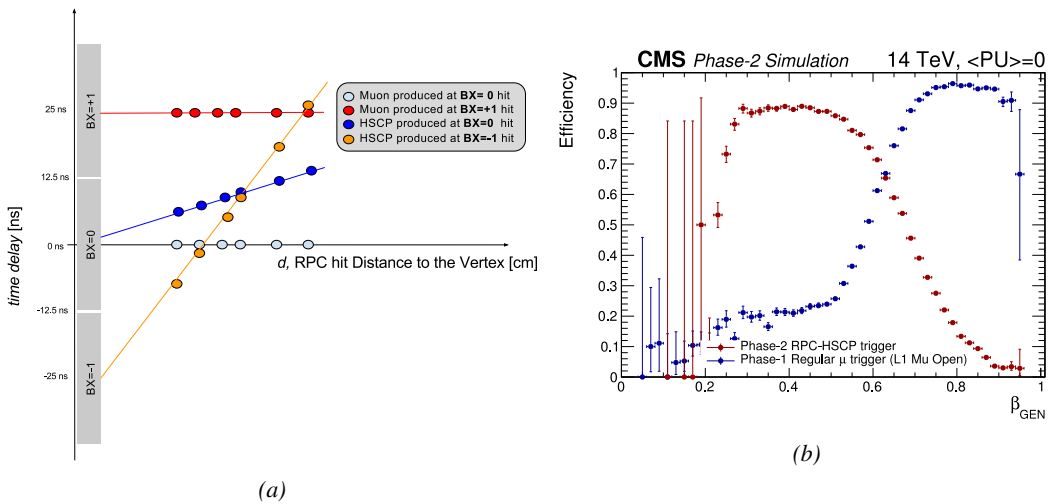


Figure 4.9: (a): Time delay with respect to a particle traveling at the speed of light measured at consecutive RPC stations for particles originating at different bunch crossings and traveling at different velocities [177]. (b): In blue is showed the standard Level-1 muon trigger efficiency as a function of β and in blue is showed the RPC-HSCP trigger efficiency after upgrade of the RPC Link System [177].

The exploitation of the full time resolution would make the synchronization of the RPC system easier and allow to have a finer offline out-of-time background removal within the 25 ns between consecutive bunch crossings. Moreover, this would greatly improve the trigger and reconstruction on HSCPs. Using the TOF information in between consecutive RPC stations, the minimal particle velocity than could be probed will drop from approximately 0.6 to 0.25 times the speed of light as showed in Figure 4.9. Upgrading RPC link system will require the installation of 1376 new link boards and 216 control boards. The new boards will make use of the recent progress made with fast FPGAs and will be a great improvement to the ASICs formerly used as they will be able to process signals from several detectors in parallel.

4.3 New detectors and increased acceptance

In the present muon system, the redundancy is assured by RPCs used for their robust bunch crossing assignments. The extension of the muon system towards higher pseudo-rapidity in an effort to complete the redundancy and to contribute to the precision of muon momentum measurements will require muon chambers with a spatial resolution less or comparable to the multiple scattering muons are subjected to while traveling through the detector volume [192].

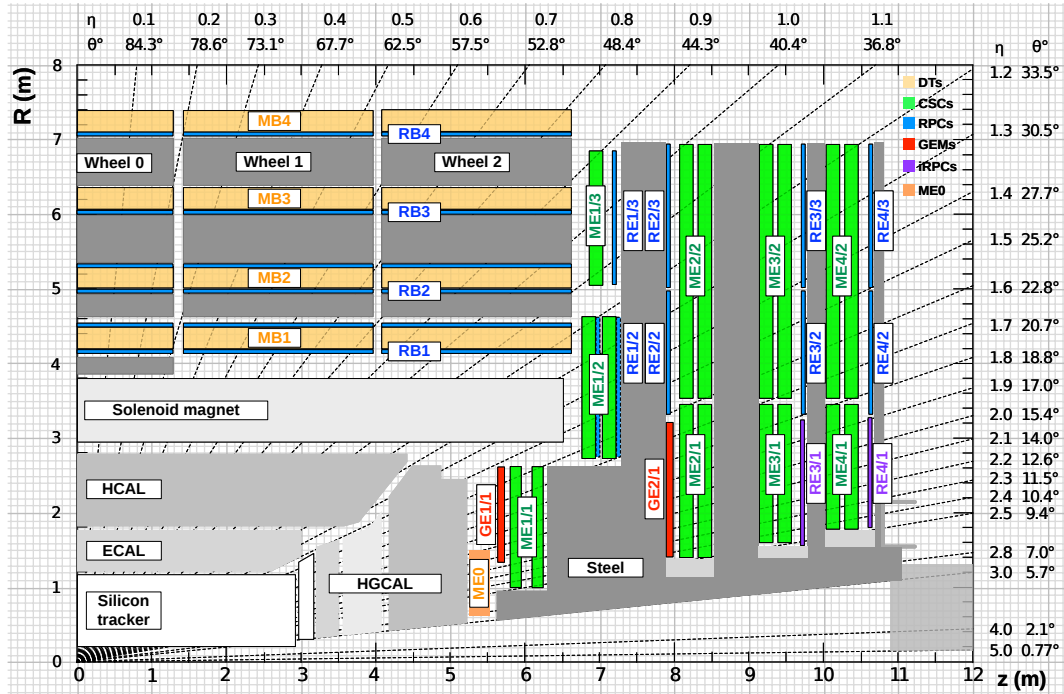
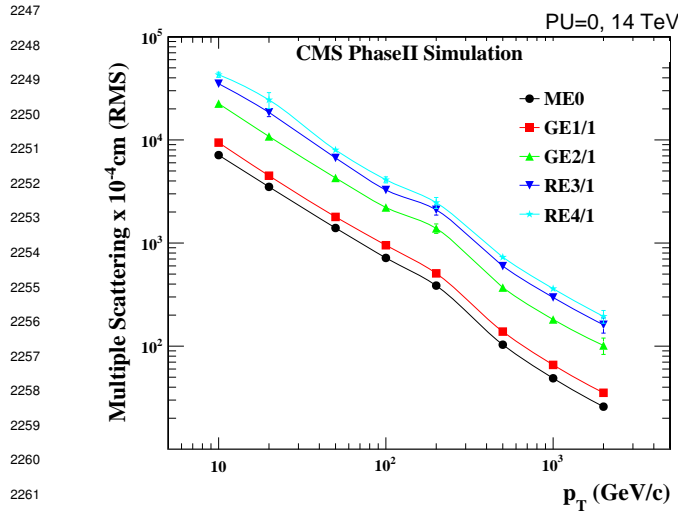


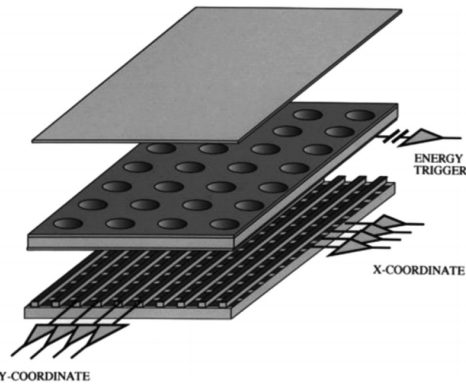
Figure 4.10: A quadrant of the muon system, showing DTs (yellow), RPCs (blue), and CSCs (green). The locations of new forward muon detectors for Phase-2 are contained within the dashed box and indicated in red for GEM stations (ME0, GE1/1, and GE2/1) and dark blue for improved RPC (iRPC) stations (RE3/1 and RE4/1).



2263 *Figure 4.11: RMS of the multiple scattering displacement as a
2264 function of muon p_T for the proposed forward muon stations. All
2265 of the electromagnetic processes such as bremsstrahlung and mag-
2266 netic field effect are included in the simulation.*

2267 showed by the simulation in Figure 4.11. Indeed, most of the plausible physics will be covered
2268 only considering muons with $p_T < 100 \text{ GeV}$.

2269 4.3.1 Gas electron multipliers



2270
2271
2272
2273
2274
2275
2276
2277
2278
2279
2280
2281
2282 *Figure 4.12: Schematics of a GEM. On top is the cathode and on the bottom, the anode on which a 2D read-
2283 out is installed. Finally, the GEM foil separates the gas
2284 volume into the drift region, in between the cathode and
2285 the foil, and the induction region, in between the foil and
2286 the anode. A negative voltage is applied on the cathode.
2287 The anode is connected to the ground.*

2288 volume is confined between two planar electrodes, the anode serving as read-out panel. The gas vol-

2247 Figure 4.10 shows a similar quadrant of CMS than the one pre-
2248 sented in Figure 2.27 with the ad-
2249 dition of Gas Electron Multiplier
2250 (GEM) (ME0, GE1/1 and GE2/1)
2251 and improved RPC (iRPC) (RE3/1
2252 and RE4/1) in the pseudo-rapidity
2253 region $1.6 < |\eta| < 2.4$. The com-
2254 pletion of the redundancy was al-
2255 ready scheduled in the original CMS
2256 Technical Proposal [252] but never
2257 addressed. The coming Phase-II
2258 is then the occasion to equip the
2259 region with the newest GEM and
2260 RPC technology. In order to match
2261 CMS requirements, a spatial reso-
2262 lution of $\mathcal{O}(\text{few mm})$ will be nec-
2263 essary for the proposed new RPC
2264 stations while the GEMs will need
2265 a resolution better than 1 mm, as

In the region closer to the interaction point where the spatial resolution is requested for the new detectors to be better than 1 mm (at least for ME0 and GE1/1 according to Figure 4.11) and where the background rate will be the highest for muon detectors, the choice has been made to use triple GEMs, micro pattern gaseous detectors, instead of the originally planned RPCs. The GE1/1 project has been the first to be approved and demonstrators have been installed in CMS already during LS1. The rest of the detectors will be installed during LS2 while the GE2/1 and ME0 projects are still under development. ME0, GE1/1 and GE2/1 will be installed respectively close to the HCAL endcap, on the first and on the second muon endcap disks as can be seen from Figure 4.10. Gas Electron Multipliers are gaseous detectors [253] whose gas

ume is divided in two or more regions by a single or multiple *GEM foils* as showed in Figure 4.12.

These foils are very thin, of the order of a few tens of μm , and are pierced with holes as can be seen in Figure 4.13. Both surfaces of the GEM foils are clad with copper in order to apply a strong electric field in between each side that will generate very strong potentials in the holes. The gas region contained in between the cathode and the GEM foil is called the drift region as the electric field is not strong enough to cause avalanches and thus start an amplification. The primary electrons drift toward the foil and are accelerated and amplified by the very high potential within the holes, as showed in Figure 4.13. Then the electrons reach the second drift region where they will induce a signal on the read-out located on the anode. By restraining the amplification process at the level of the holes, the electrons can stay confined in a very little space and thus induce a very localized current, providing the GEMs with a very good spatial resolution. The process can be repeated several times in a row, in order to achieve a stronger amplification. The GEMs that will be used in CMS are triple-GEM detectors operated with a 70/30 gas mixture of Ar/CO_2 . They contain three GEM foils and hence three electron amplifications, as can be seen in Figure 4.14.

The GEM foils used in CMS are 50 μm foils clad with 5 μm of copper on each side. The foils are pierced with double-canonical holes which inner and outer diameters are respectively 50 and 70 μm which are placed 140 μm from each other in a hexagonal pattern, as showed in Figure 4.13. These detectors have a time resolution better than 10 ns and reach very good spatial resolutions of less than 200 μrad as indeed the position of the hits is not measured along the strips but following the azimuthal angle granularity of the radially organized trapezoidal strips.

The GEM Upgrade project started with GE1/1 [254]. GE1/1 detectors will already be installed

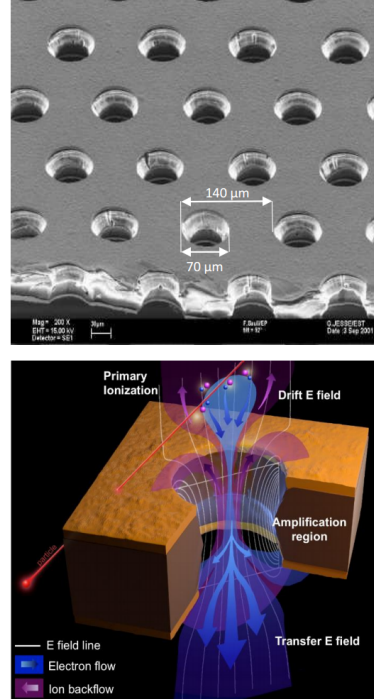


Figure 4.13: Top: Picture of a CMS GEM foil provided by a scanning electron microscope. Bottom: Representation of the electric field in a GEM hole and of the amplification electrons and ions undergo due to the very intense electric field.

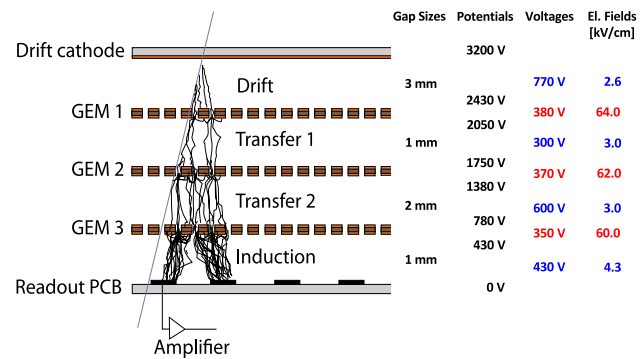


Figure 4.14: The gas volume of CMS triple-GEMs is divided into four areas. Primary electrons are created in the Drift area and amplified by three GEM-foils while drifting through Transfer areas. Reaching the Induction area, the avalanche induces current in the read-out. The typical dimensions and potentials are provided.

2336 during LS2. GE2/1 and ME0, on the other hand, will profit of the R&D knowledge and skills
 2337 developed for GE1/1 while the requirements for each subsystem are different as they are not placed
 2338 at the same distance from the interaction point. In this very forward region, a different position with
 2339 respect to the center of the detector can dramatically change the conditions in which the detectors
 2340 will have to be operated. In terms of rate capability, GE2/1, which is the furthest, is required to
 2341 withstand 2.1 kHz/cm^2 while GE1/1 needs to be better than 10 kHz/cm^2 and ME0, better than
 2342 150 kHz/cm^2 . In terms of ageing with respect to charge deposition, ME0 needs to be certified to
 2343 840 mC/cm^2 , GE1/1 to 200 mC/cm^2 and GE2/1 only to 9 mC/cm^2 . All 3 detectors need to have a
 2344 time resolution better than 10 ns and an angular resolution better than $500 \mu\text{rad}$.

2345 On each GE1/1 ring, 36 super chambers, consisting of two single GEM layers and spanning 10° ,
 2346 will be installed covering the pseudo-rapidity region $1.6 < |\eta| < 2.2$ together with ME1/1 CSCs.
 2347 The reach of the muon system will be improved thanks to the GE2/1 that will overlap with the GE1/1
 2348 and cover a region from $|\eta| > 1.6$ to $|\eta| < 2.4$ and complete the redundancy of ME2/1. The super
 2349 chambers, built with two triple-GEM layers each consisting of four single GEM modules due to
 2350 the rather large surface of the GE2/1 chambers, that will be installed on the first ring of the second
 2351 endcap will span 20° each. Hence, a total of 72 chambers will be assembled to equip the muon
 2352 system. Finally, the ME0 installed near the HCAL endcap will cover the region $2.0 < |\eta| < 2.8$.
 2353 This subsystem will consist in super modules of six layers of triple-GEM detectors covering an
 2354 azimuthal angle of 20° leading to the construction of 216 single detectors.

2355 Adding the GEMs into the forward region of the muon system will allow to strongly enhance
 2356 the Level-1 Trigger performance as shown in Figure 4.15. In the region $1.6 < |\eta| < 2.4$, the trigger
 2357 efficiency of the current system would lie between 80 and 90% under HL-LHC conditions. The
 2358 installation of GEMs would bring the efficiency to a consistent 92 to 94% on the entire region. At
 2359 the same time, the trigger rate is expected to fluctuate from 3 to 10 kHz with the current system
 2360 alone. The addition of detectors to complete the redundancy would allow keeping the rate mostly
 2361 under 2 kHz. Moreover, benefiting from the good spatial and angular resolution of the GEMs, the
 2362 precision into the muon measurement will also be improved by an order of magnitude thanks to the
 2363 addition of GEMs as can be seen from the simulation presented in Figure 4.16.

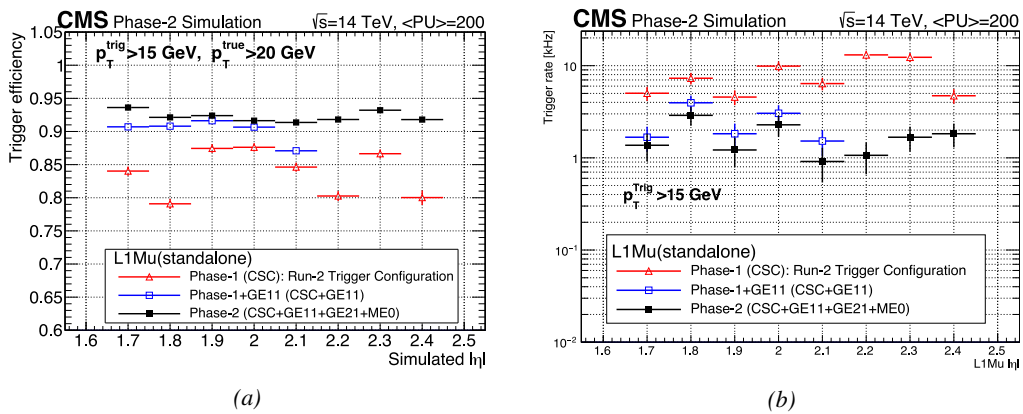


Figure 4.15: Simulated (a) efficiency and (b) rate of the standalone Level-1 muon trigger using tracks reconstructed in CSCs and all GEM stations compared with Phase-I values in the case where only CSCs are used or CSCs+GE1/1. The zones of inefficiency of the CSC subsystem are compensated by the addition of GEMs during Phase-2 and the trigger rates is kept from increasing due to the high luminosity [177].

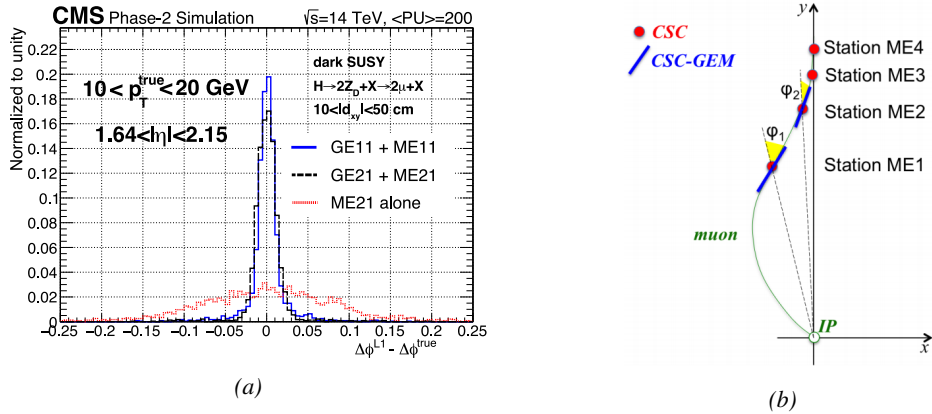


Figure 4.16: (a): Simulated resolution of the muon direction measurement $\Delta\phi$ with Phase-2 conditions. In the second endcap station, the resolution is compared in the case of CSCs (ME2/1) alone and CSCs+GEMs (GE2/1+ME2/1) while a similar resolution measurement is given in the case of the first station (GE1/1+ME1/1) [177]. (b): The addition of GEM detectors on stations 1 and 2 (ME0 is considered to contribute to station 1) as redundant system to CSCs allows improving the muon momentum improvement through a more accurate measurement of the local bending angles ϕ_1 and ϕ_2 [177].

2364 4.3.2 Improved forward resistive plate chambers

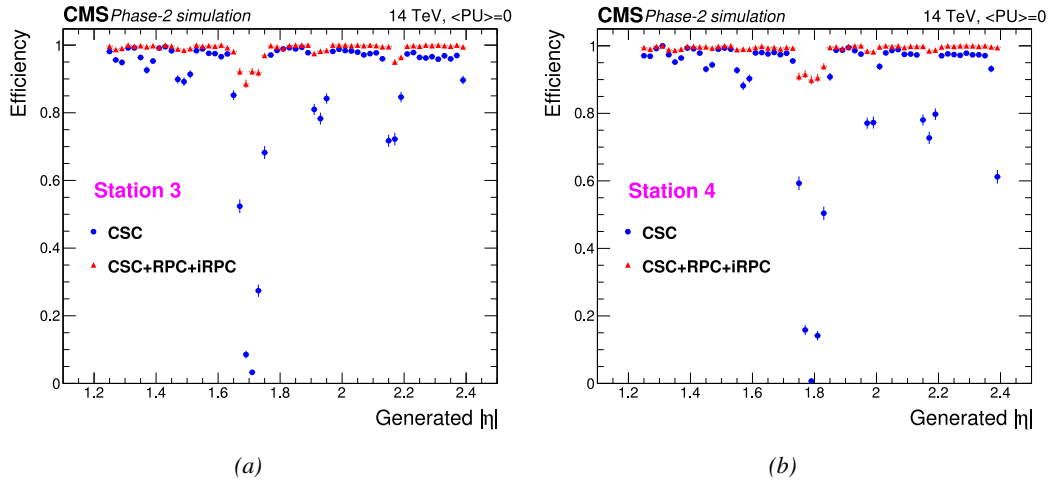


Figure 4.17: Simulation of the impact of RPC hit inclusion onto the local trigger primitive efficiency in station 3 (a) and station 4 (b) [177]. The contribution of iRPC starts above $|\eta| = 1.8$.

2365 Figure 4.10 shows that the iRPCs that will equip the third and fourth endcap disks in position RE3/1
 2366 and RE4/1 will finally be the partners of the CSCs in position ME3/1 and ME4/1. They will complete
 2367 Phase-1 plans by bringing the needed upgrades in the perspective of Phase-2 as the older chambers
 2368 are not suitable to equip the forward region of CMS due to HL-LHC rates and charge deposition.
 2369 By completing the redundancy, more hits along the muon track will be available and the lever arm
 2370 will be improved. The benefits from extending the redundancy of the muon system with iRPCs to

the forward most region is shown in Figure 4.17 in which the trigger efficiency is presented with and without RPCs. It is possible to see that the efficiency of the CMS muon trigger with the complete redundancy is consistently improved to a level above 95% in the region $|\eta| > 1.8$ as the iRPCs help filling the holes in the CSC system.

The detectors that will be installed in the coming years will have similarities with the already existing RPC system. 18 of the new chambers, each spanning 20° in φ around the beam axis with 96 radially oriented trapezoidal read-out strips, will cover each muon endcap disk leading to the production of 72 iRPCs. The main difference with the old RPC detectors will be found at the level of the read-out panels. Indeed, the new chambers will not feature read-out strips segmented in η but rather will favor a read-out on both strip ends to determine the position of the hits along the chamber. By using fast front-end electronics a radial spatial resolution of the order of 2 cm could be achieved to contribute to the better reconstruction of muons in the forward region where the bending due to the magnetic field is low. This technical choice is motivated by the fact that, in the case a η segmentation were to be used, at least five pseudo-rapidity partitions would have been necessary to reach the minimal radial spatial resolution (≈ 20 cm). Having only one strip along the chamber read-out from both ends reduces by 60% the total number of channels and the necessary cabling, and allows for a better spatial resolution. The strip pitch will range from 6.0 mm (5.9 mm) on the high pseudo-rapidity end to 12.3 mm (10.9 mm) on the low one on position RE3/1 (RE4/1). The spatial resolution in the direction perpendicular to the strips should reach approximately 3 mm, better than the minimal needed resolution (Figure 4.11). Finally, the overall time resolution of the new installation will be equally 1 ns, as for the present due to the same link system being used even though the detector itself can achieve a time resolution of less than 100 ps, necessary for a spatial reconstruction of the hits with a resolution of 2 cm or less along the strip length.

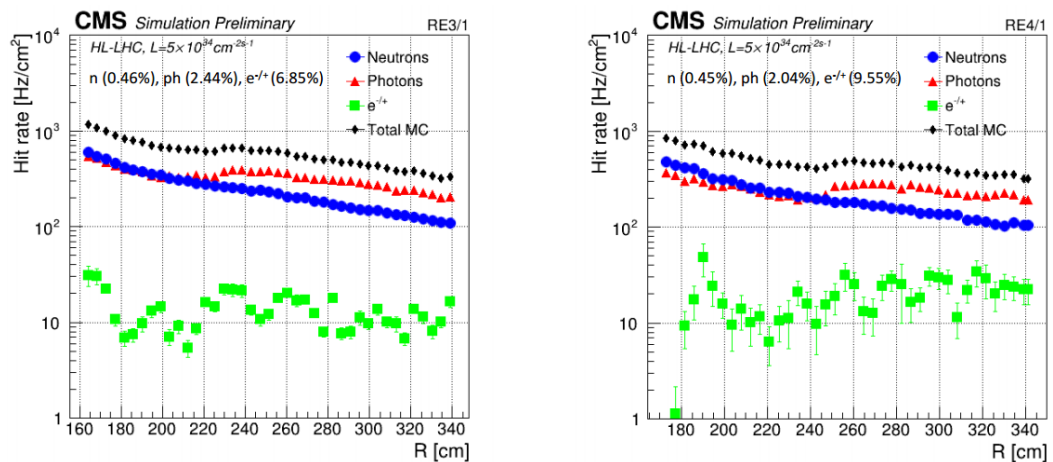


Figure 4.18: Expected hit rate due to neutrons, photons, electrons and positrons at HL-HLC instantaneous luminosity of $5 \times 10^{34} \text{ cm}^{-2}\text{s}^{-1}$ in RE3/1 and RE4/1 chambers [255, 256]. The sensitivities of iRPCs used in the simulation for each particle are reported and differ from one endcap disk to another as the energies of the considered particles varies with the increasing distance from the interaction point.

Having only a single strip instead of pseudo-rapidity segmentation will increase the probability of double hits in the same channel. The probability was estimated to be low enough as it shouldn't exceed 0.7%. This estimation was made assuming an average hit rate per unit area of 600 Hz/cm²

in the iRPCs (see Figure 4.18), a cluster size (average number of strips fired per muon) of 2, a strip active area of $158.4 \times 0.87 \text{ cm}^2$ and a safety factor 3. The corresponding rate per strip is estimated to be 380 kHz leading to an average time interval in between two consecutive hits of 2600 ns. This is compared to the minimal time interval of 16 ns necessary to avoid ambiguities. Indeed, a maximum of 10 ns is spent by the signal traveling through the strip to reach the electronics to which can be added 1 ns of dead time and 2 Time-to-Digital Converter (TDC) clock cycles of 2.5 ns to convert the signal arrival time into a digital value in the FEEs. The probability of having ambiguous double hits in a strip is then the ratio between the minimal time interval in between two consecutive hits and the average time interval estimated from the rate the detectors would be subjected to.

The instantaneous luminosity at HL-LHC being very high, the rates at the position of the new chambers needed to be simulated in order to understand the necessary requirements for these detectors. The simulated results for different background components (neutrons, photons, electrons and positrons) are shown in Figure 4.18 assuming known sensitivities to these particles. It is shown that on average over the iRPC areas the rates would be of the order of 600 Hz/cm^2 (600 Hz/cm^2 seen in RE3/1 and 480 Hz/cm^2 in RE4/1) [255, 256]. Thus, taking into account a safety factor of about 3, it was decided that improved RPCs should at least be certified for rates reaching 2 Hz/cm^2 which will be achieved thanks to several improvements on the design and on the electronics. The detectors design will be based on the existing RPCs as they will also feature double RPC gaps. Similarly to the existing RPC system, the electrode material will be HPL although the thickness of the electrodes and of the gas gap will be reduced to 1.4 mm as a thinner gas gap leads to a decrease of deposited charge per avalanche as showed in Figure 4.19. The charge deposition in the case of a 1.4 mm thick gas gap is reduced by a factor greater than 5 when compared to a 2 mm gas gap at a similar electric field. The smaller the gas gap, the more the detector becomes sensitive to gap non-uniformities across the electrode planes, making a gap of 1.4 mm a good compromise in between these two competing factors.

A lower charge deposition inside of the detector volume means a slower ageing and a longer lifetime for detectors subjected to high irradiation. But, in order to take advantage of the lower detector gain, more sensitive electronics are required such that part of the gain that was formerly achieved in the gas volume can be moved to the electronics. Achieving this with the technology developed more than ten years ago for the present system is not possible as the signal over noise ratio of such electronics doesn't allow to detect charges as low as 10 fC. Moreover, the new front-end electronics will need to be radiation hard to survive more than ten years of HL-LHC conditions. The new technology that has been chosen is based on the PETIROC ASIC manufactured by OMEGA and is a 64-channel ASIC called CMS RPCROC[177, 257, 258]. The properties of these electronics will be discussed in Chapter 6.

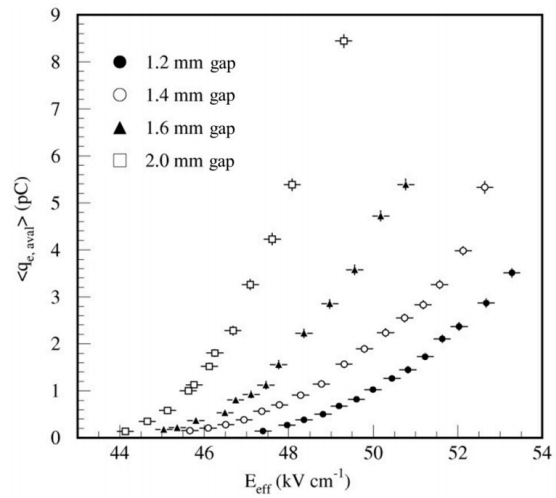
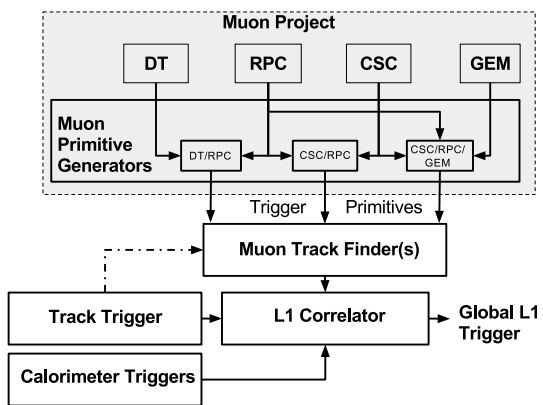


Figure 4.19: Measured average charge per avalanche as a function of the effective electric field for different gas gap thickness in double-gap RPCs using HPL electrodes [177].

2443 4.4 Impact on Level-1 Trigger and physics performance



2444
2445
2446
2447
2448
2449
2450
2451
2452
2453
2454
2455
2456
2457
2458
2459
2460
2461
2462
2463
2464
2465
2466
2467
2468
2469
2470
2471
2472
2473
2474
2475
2476
2477
2478
2479
2480
2481
2482
2483
2484
2485
2486
2487
2488
2489
2490
2491
2492
2493
2494
2495
2496
2497
2498
2499
2500
2501
2502
2503
2504
2505
2506
2507
2508
2509
2510
2511
2512
2513
2514
2515
2516
2517
2518
2519
2520
2521
2522
2523
2524
2525
2526
2527
2528
2529
2530
2531
2532
2533
2534
2535
2536
2537
2538
2539
2540
2541
2542
2543
2544
2545
2546
2547
2548
2549
2550
2551
2552
2553
2554
2555
2556
2557
2558
2559
2560
2561
2562
2563
2564
2565
2566
2567
2568
2569
2570
2571
2572
2573
2574
2575
2576
2577
2578
2579
2580
2581
2582
2583
2584
2585
2586
2587
2588
2589
2590
2591
2592
2593
2594
2595
2596
2597
2598
2599
2600
2601
2602
2603
2604
2605
2606
2607
2608
2609
2610
2611
2612
2613
2614
2615
2616
2617
2618
2619
2620
2621
2622
2623
2624
2625
2626
2627
2628
2629
2630
2631
2632
2633
2634
2635
2636
2637
2638
2639
2640
2641
2642
2643
2644
2645
2646
2647
2648
2649
2650
2651
2652
2653
2654
2655
2656
2657
2658
2659
2660
2661
2662
2663
2664
2665
2666
2667
2668
2669
2670
2671
2672
2673
2674
2675
2676
2677
2678
2679
2680
2681
2682
2683
2684
2685
2686
2687
2688
2689
2690
2691
2692
2693
2694
2695
2696
2697
2698
2699
2700
2701
2702
2703
2704
2705
2706
2707
2708
2709
2710
2711
2712
2713
2714
2715
2716
2717
2718
2719
2720
2721
2722
2723
2724
2725
2726
2727
2728
2729
2730
2731
2732
2733
2734
2735
2736
2737
2738
2739
2740
2741
2742
2743
2744
2745
2746
2747
2748
2749
2750
2751
2752
2753
2754
2755
2756
2757
2758
2759
2760
2761
2762
2763
2764
2765
2766
2767
2768
2769
2770
2771
2772
2773
2774
2775
2776
2777
2778
2779
2780
2781
2782
2783
2784
2785
2786
2787
2788
2789
2790
2791
2792
2793
2794
2795
2796
2797
2798
2799
2800
2801
2802
2803
2804
2805
2806
2807
2808
2809
2810
2811
2812
2813
2814
2815
2816
2817
2818
2819
2820
2821
2822
2823
2824
2825
2826
2827
2828
2829
2830
2831
2832
2833
2834
2835
2836
2837
2838
2839
2840
2841
2842
2843
2844
2845
2846
2847
2848
2849
2850
2851
2852
2853
2854
2855
2856
2857
2858
2859
2860
2861
2862
2863
2864
2865
2866
2867
2868
2869
2870
2871
2872
2873
2874
2875
2876
2877
2878
2879
2880
2881
2882
2883
2884
2885
2886
2887
2888
2889
2890
2891
2892
2893
2894
2895
2896
2897
2898
2899
2900
2901
2902
2903
2904
2905
2906
2907
2908
2909
2910
2911
2912
2913
2914
2915
2916
2917
2918
2919
2920
2921
2922
2923
2924
2925
2926
2927
2928
2929
2930
2931
2932
2933
2934
2935
2936
2937
2938
2939
2940
2941
2942
2943
2944
2945
2946
2947
2948
2949
2950
2951
2952
2953
2954
2955
2956
2957
2958
2959
2960
2961
2962
2963
2964
2965
2966
2967
2968
2969
2970
2971
2972
2973
2974
2975
2976
2977
2978
2979
2980
2981
2982
2983
2984
2985
2986
2987
2988
2989
2990
2991
2992
2993
2994
2995
2996
2997
2998
2999
3000
3001
3002
3003
3004
3005
3006
3007
3008
3009
3010
3011
3012
3013
3014
3015
3016
3017
3018
3019
3020
3021
3022
3023
3024
3025
3026
3027
3028
3029
3030
3031
3032
3033
3034
3035
3036
3037
3038
3039
3040
3041
3042
3043
3044
3045
3046
3047
3048
3049
3050
3051
3052
3053
3054
3055
3056
3057
3058
3059
3060
3061
3062
3063
3064
3065
3066
3067
3068
3069
3070
3071
3072
3073
3074
3075
3076
3077
3078
3079
3080
3081
3082
3083
3084
3085
3086
3087
3088
3089
3090
3091
3092
3093
3094
3095
3096
3097
3098
3099
3100
3101
3102
3103
3104
3105
3106
3107
3108
3109
3110
3111
3112
3113
3114
3115
3116
3117
3118
3119
3120
3121
3122
3123
3124
3125
3126
3127
3128
3129
3130
3131
3132
3133
3134
3135
3136
3137
3138
3139
3140
3141
3142
3143
3144
3145
3146
3147
3148
3149
3150
3151
3152
3153
3154
3155
3156
3157
3158
3159
3160
3161
3162
3163
3164
3165
3166
3167
3168
3169
3170
3171
3172
3173
3174
3175
3176
3177
3178
3179
3180
3181
3182
3183
3184
3185
3186
3187
3188
3189
3190
3191
3192
3193
3194
3195
3196
3197
3198
3199
3200
3201
3202
3203
3204
3205
3206
3207
3208
3209
3210
3211
3212
3213
3214
3215
3216
3217
3218
3219
3220
3221
3222
3223
3224
3225
3226
3227
3228
3229
3230
3231
3232
3233
3234
3235
3236
3237
3238
3239
3240
3241
3242
3243
3244
3245
3246
3247
3248
3249
3250
3251
3252
3253
3254
3255
3256
3257
3258
3259
3260
3261
3262
3263
3264
3265
3266
3267
3268
3269
3270
3271
3272
3273
3274
3275
3276
3277
3278
3279
3280
3281
3282
3283
3284
3285
3286
3287
3288
3289
3290
3291
3292
3293
3294
3295
3296
3297
3298
3299
3300
3301
3302
3303
3304
3305
3306
3307
3308
3309
3310
3311
3312
3313
3314
3315
3316
3317
3318
3319
3320
3321
3322
3323
3324
3325
3326
3327
3328
3329
3330
3331
3332
3333
3334
3335
3336
3337
3338
3339
3340
3341
3342
3343
3344
3345
3346
3347
3348
3349
3350
3351
3352
3353
3354
3355
3356
3357
3358
3359
3360
3361
3362
3363
3364
3365
3366
3367
3368
3369
3370
3371
3372
3373
3374
3375
3376
3377
3378
3379
3380
3381
3382
3383
3384
3385
3386
3387
3388
3389
3390
3391
3392
3393
3394
3395
3396
3397
3398
3399
3400
3401
3402
3403
3404
3405
3406
3407
3408
3409
3410
3411
3412
3413
3414
3415
3416
3417
3418
3419
3420
3421
3422
3423
3424
3425
3426
3427
3428
3429
3430
3431
3432
3433
3434
3435
3436
3437
3438
3439
3440
3441
3442
3443
3444
3445
3446
3447
3448
3449
3450
3451
3452
3453
3454
3455
3456
3457
3458
3459
3460
3461
3462
3463
3464
3465
3466
3467
3468
3469
3470
3471
3472
3473
3474
3475
3476
3477
3478
3479
3480
3481
3482
3483
3484
3485
3486
3487
3488
3489
3490
3491
3492
3493
3494
3495
3496
3497
3498
3499
3500
3501
3502
3503
3504
3505
3506
3507
3508
3509
3510
3511
3512
3513
3514
3515
3516
3517
3518
3519
3520
3521
3522
3523
3524
3525
3526
3527
3528
3529
3530
3531
3532
3533
3534
3535
3536
3537
3538
3539
3540
3541
3542
3543
3544
3545
3546
3547
3548
3549
3550
3551
3552
3553
3554
3555
3556
3557
3558
3559
3560
3561
3562
3563
3564
3565
3566
3567
3568
3569
3570
3571
3572
3573
3574
3575
3576
3577
3578
3579
3580
3581
3582
3583
3584
3585
3586
3587
3588
3589
3590
3591
3592
3593
3594
3595
3596
3597
3598
3599
3600
3601
3602
3603
3604
3605
3606
3607
3608
3609
3610
3611
3612
3613
3614
3615
3616
3617
3618
3619
3620
3621
3622
3623
3624
3625
3626
3627
3628
3629
3630
3631
3632
3633
3634
3635
3636
3637
3638
3639
3640
3641
3642
3643
3644
3645
3646
3647
3648
3649
3650
3651
3652
3653
3654
3655
3656
3657
3658
3659
3660
3661
3662
3663
3664
3665
3666
3667
3668
3669
3670
3671
3672
3673
3674
3675
3676
3677
3678
3679
3680
3681
3682
3683
3684
3685
3686
3687
3688
3689
3690
3691
3692
3693
3694
3695
3696
3697
3698
3699
3700
3701
3702
3703
3704
3705
3706
3707
3708
3709
3710
3711
3712
3713
3714
3715
3716
3717
3718
3719
3720
3721
3722
3723
3724
3725
3726
3727
3728
3729
3730
3731
3732
3733
3734
3735
3736
3737
3738
3739
3740
3741
3742
3743
3744
3745
3746
3747
3748
3749
3750
3751
3752
3753
3754
3755
3756
3757
3758
3759
3760
3761
3762
3763
3764
3765
3766
3767
3768
3769
3770
3771
3772
3773
3774
3775
3776
3777
3778
3779
3780
3781
3782
3783
3784
3785
3786
3787
3788
3789
3790
3791
3792
3793
3794
3795
3796
3797
3798
3799
3800
3801
3802
3803
3804
3805
3806
3807
3808
3809
3810
3811
3812
3813
3814
3815
3816
3817
3818
3819
3820
3821
3822
3823
3824
3825
3826
3827
3828
3829
3830
3831
3832
3833
3834
3835
3836
3837
3838
3839
3840
3841
3842
3843
3844
3845
3846
3847
3848
3849
3850
3851
3852
3853
3854
3855
3856
3857
3858
3859
3860
3861
3862
3863
3864
3865
3866
3867
3868
3869
3870
3871
3872
3873
3874
3875
3876
3877
3878
3879
3880
3881
3882
3883
3884
3885
3886
3887
3888
3889
3890
3891
3892
3893
3894
3895
3896
3897
3898
3899
3900
3901
3902
3903
3904
3905
3906
3907
3908
3909
3910
3911
3912
3913
3914
3915
3916
3917
3918
3919
3920
3921
3922
3923
3924
3925
3926
3927
3928
3929
3930
3931
3932
3933
3934
3935
3936
3937
3938
3939
3940
3941
3942
3943
3944
3945
3946
3947
3948
3949
3950
3951
3952
3953
3954
3955
3956
3957
3958
3959
3960
3961
3962
3963
3964
3965
3966
3967
3968
3969
3970
3971
3972
3973
3974
3975
3976
3977
3978
3979
3980
3981
3982
3983
3984
3985
3986
3987
3988
3989
3990
3991
3992
3993
3994
3995
3996
3997
3998
3999
4000
4001
4002
4003
4004
4005
4006
4007
4008
4009
4010
4011
4012
4013
4014
4015
4016
4017
4018
4019
4020
4021
4022
4023
4024
4025
4026
4027
4028
4029
4030
4031
4032
4033
4034
4035
4036
4037
4038
4039
4040
4041
4042
4043
4044
4045
4046
4047
4048
4049
4050
4051
4052
4053
4054
4055
4056
4057
4058
4059
4060
4061
4062
4063
4064
4065
4066
4067
4068
4069
4070
4071
4072
4073
4074
4075
4076
4077
4078
4079
4080
4081
4082
4083
4084
4085
4086
4087
4088
4089
4090
4091
4092
4093
4094
4095
4096
4097
4098
4099
4100
4101
4102
4103
4104
4105
4106
4107
4108
4109
4110
4111
4112
4113
4114
4115
4116
4117
4118
4119
4120
4121
4122
4123
4124
4125
4126
4127
4128
4129
4130
4131
4132
4133
4134
4135
4136
4137
4138
4139
4140
4141
4142
4143
4144
4145
4146
4147
4148
4149
4150
4151
4152
4153
4154
4155
4156
4157
4158
4159
4160
4161
4162
4163
4164
4165
4166
4167
4168
4169
4170
4171
4172
4173
4174
4175
4176
4177
4178
4179
4180
4181
4182
4183
4184
4185
4186
4187
4188
4189
4190
4191
4192
4193
4194
4195
4196
4197
4198
4199
4200
4201
4202
4203
4204
4205
4206
4207
4208
4209
4210
4211
4212
4213
4214
4215
4216
4217
4218
4219
4220
4221
4222
4223
4224
4225
4226
4227
4228
4229
4230
4231
4232
4233
4234
4235
4236
4237
4238
4239
4240
4241
4242
4243
4244

most challenging pseudo-rapidity region. Indeed, the contribution from the GEMs to the lever arm of each track thanks to their high angular resolution will be a great asset in achieving such results, as can be seen in Figure 4.23. The rate will be partly reduced in the forward region thanks to the better spatial resolution of iRPCs, with respect to the current RPC system. The ambiguity brought by multiple local charged tracks in CSCs will be reduced, as explained through Figure 4.24. Indeed, as the rates will increase, the probability to record more than a single local charged track will greatly increase. This is due to the fact that the trigger algorithm uses information from three consecutive bunch crossings to find muon tracks. It is estimated that with iRPCs operated at 95% efficiency the resolution of ambiguous events would be of the order of 99.7%.

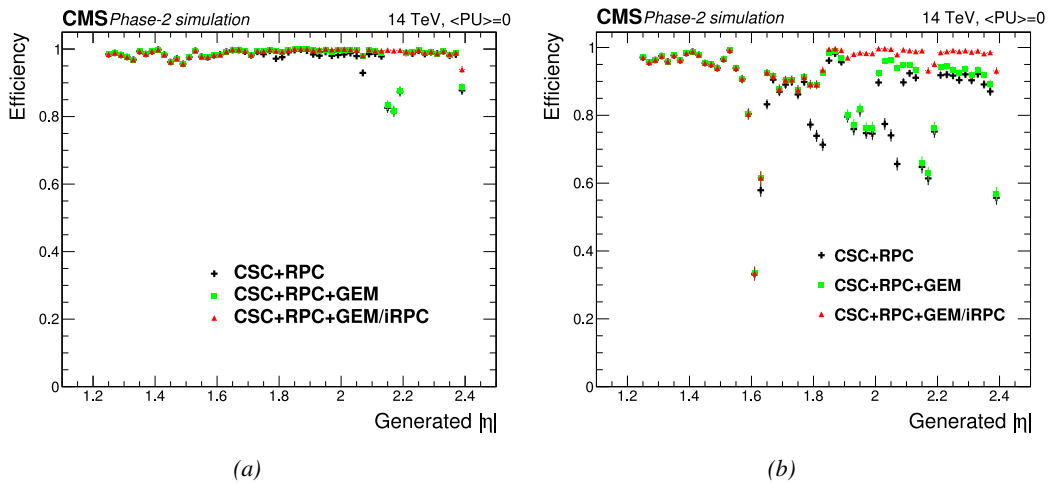


Figure 4.21: Efficiency of the L1 trigger in the endcap region after Phase-2 upgrade in the case CSC/GEM/RPC hits are requested in at least two stations out of four (a) and in all four stations (b) [177].

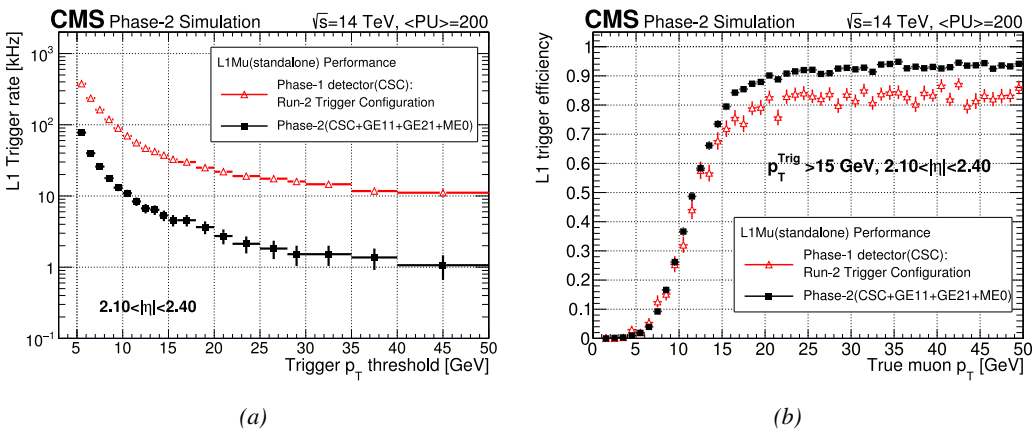


Figure 4.22: Comparison of L1 trigger performances for prompt muons with and without the addition of GEMs in the region $2.1 < |\eta| < 2.4$ at Phase-2 conditions [177]. GEMs would allow a reduction of the trigger accept rate by an order of magnitude (a) while increasing the trigger efficiency (b).

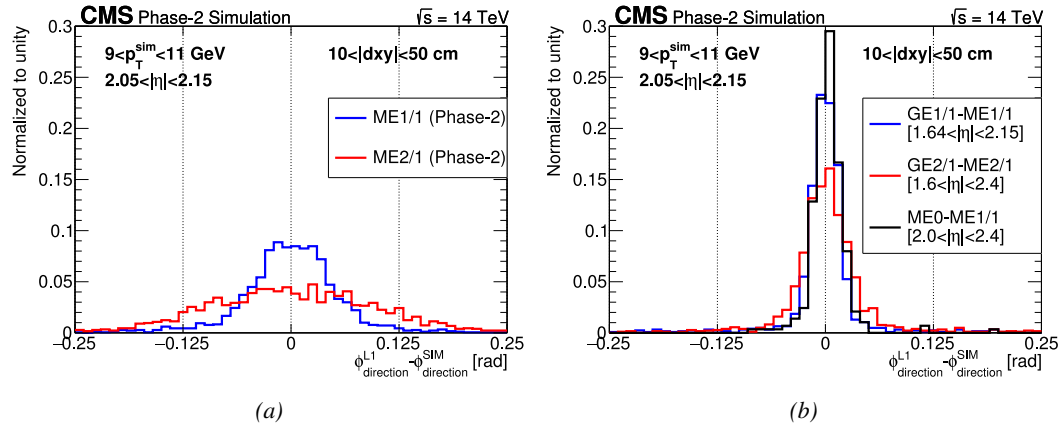


Figure 4.23: The angular resolution on reconstructed muon tracks in the GEM overlap region $2.0 < |\eta| < 2.15$ is compared for Phase-2 conditions in the case CSC are alone (a) and in the case the GEMs' data, including ME0, is combined to which of CSCs (b) [177].

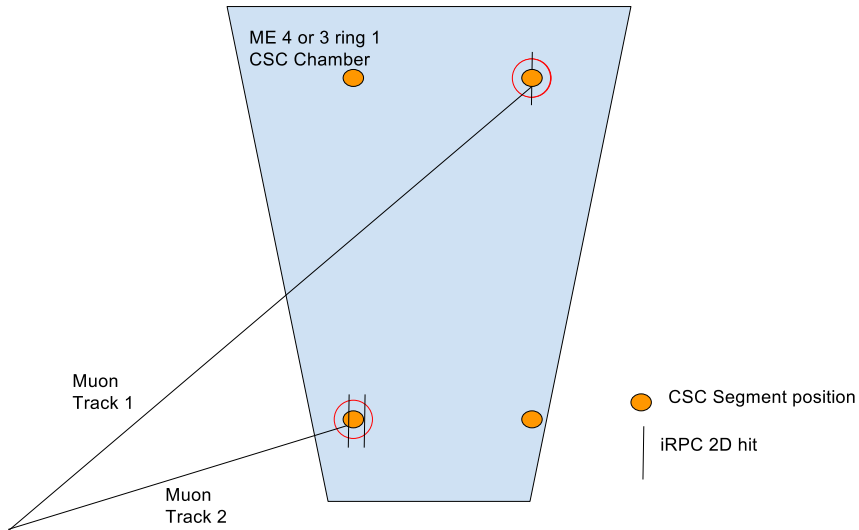


Figure 4.24: Resolution of the LCT ambiguous events thanks to the combination of CSC and iRPC readout data. Using CSCs only, two pairs of hits are possible [177].

4.5 Ecofriendly gas studies

In the last steps of R&D, the gas mixture of CMS RPCs was foreseen to be a 96.2/3.5/0.3 composition of $C_2H_2F_4/i-C_4H_{10}/SF_6$ [205] but finally it was slightly changed into a 95.2/4.5/0.3 mixture of the same gases [260]. A summary of the operation performance of the RPCs since the start of LHC and of CMS data taking is given in Figure 4.25 [261]. The performance of the detectors is regularly monitored and the operating voltages updated in order to obtain a very stable performance through time. Nevertheless, the detectors will face new challenges during Phase-II during which they will be exposed to more extreme radiation conditions. Description of the longevity tests with extreme

irradiation and the conclusions regarding the operation of the present RPC system will be given in Chapter 5.

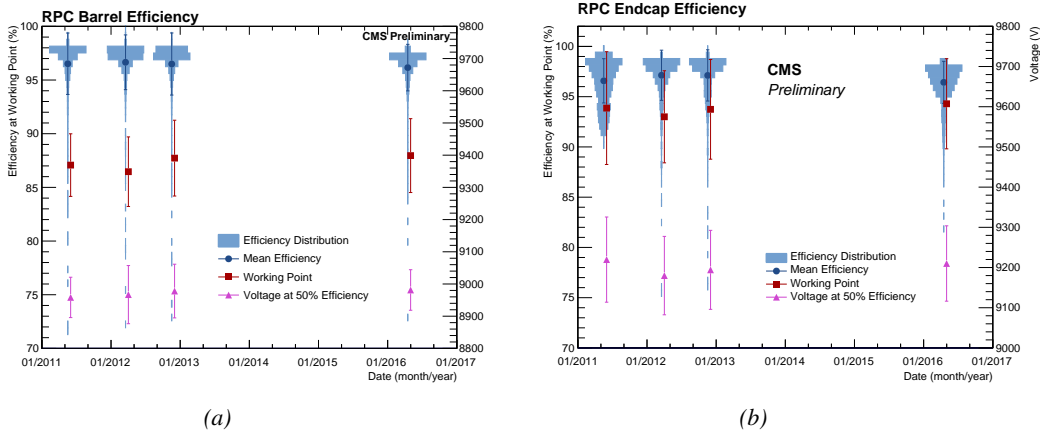


Figure 4.25: Evolution of the efficiency, working voltage, and voltage at 50% of maximum efficiency for CMS Barrel (a) and Endcap (b) RPCs obtained through yearly voltage scans since 2011. The working voltage of each RPC is updated after each voltage scan to ensure optimal operation [261].

It was already discussed that in the future, it is likely that the use of freon gases could be banned. Using CF_4 , $C_2H_2F_4$ and SF_6 , both CSC and RPC subsystems will need to address this problem by finding new gas mixture for the operation of their detectors. Finding a replacement for these gas components that were used for very specific reasons is a great challenge. Indeed, CSCs use CF_4 in order to enhance the longevity of the detectors, increase the drift velocity of electrons and quench photons with a non-flammable gas mixture. RPCs use a mixture mainly composed of $C_2H_2F_4$, or $R134a$, that features a high effective Townsend coefficient and the great average fast charge allowing for operations with a high threshold. The mixture also contains a small fraction of SF_6 that is used for its electronegative properties that prevents the development of delta-rays in the gas volume that might trigger multiple ionization and avalanches. It only represents 0.3% of CMS standard mixture but more than 5% of its overall GWP.

	CSC	RPC
Greenhouse gases used	CF_4	$C_2H_2F_4$ and SF_6
Greenhouse gases fraction in the gas mixture	10%	95.2% and 0.3%
Global Warming Potential (relative to CO_2)	6500	1300 and 23900
Gas mixture re-circulation	Yes, 90%	Yes, 85%
Gas mixture replenishing rate (l/hr)	700	1100
F-gas recuperation	Yes, $\approx 40\%$	No
F-gas venting rate (l/hr)	42	1047 and 3.3
CO_2 -equivalent rate (m^3/h)	273	1440
Relative impact (entire muon system = 100%)	16%	84%

Table 4.1: Details of the greenhouse fluorinated gases used in CMS and of their GWP [177].

All these gases have a very high GWP, as reported in Table 4.1, and only few options are left. The subsystems need to work on strongly decreasing the loss of these gases due to leaks in the gas system

or need to completely change their gas mixture for more ecofriendly ones. Reducing the amount of F-gas released in the atmosphere due to leaks on the current gas system will require installation of a F-gas recuperation system on RPCs side and an upgrade of CSCs existing one in addition to the repair of existing leaks. With such measures, it is expected that the total rate of greenhouses gas vented in the atmosphere would represent only 1.6% of the current levels [177]. In the most critical case the F-gas were to be banned, it would be necessary to have replacement mixtures to operate CMS. CSC is presently investigating replacement for CF_4 such as CF_3I , C_4F_6 , IC_3F_6 , C_3F_8 or CHF_3 . RPCs, in collaboration with the ATLAS RPC group which uses the same gas mixture, have identified CF_3I ($GWP \leq 1$) and $C_3H_2F_4$ ($GWP \sim 6$), referred to as *HFO-1234ze*, as potential candidates with mixtures containing CO_2 . CO_2 is already widely used by various RPC experiments in mixtures with argon. More R&D needs to be conducted for both subsystems before concluding on the best alternative. Finding no good alternative to the present mixtures will require very efficient abatement system in CMS to burn and convert the greenhouse gases into less harmful ones. This way, the air pollution would be strongly reduced.

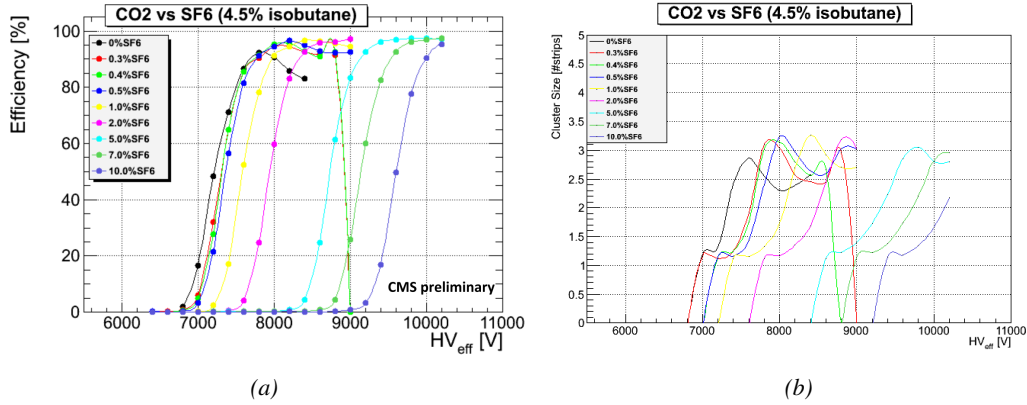


Figure 4.26: Efficiency (a) [203] and cluster size (b) of a standard double-gap RPC operated with CO_2 mixtures for different ratios of SF_6 .

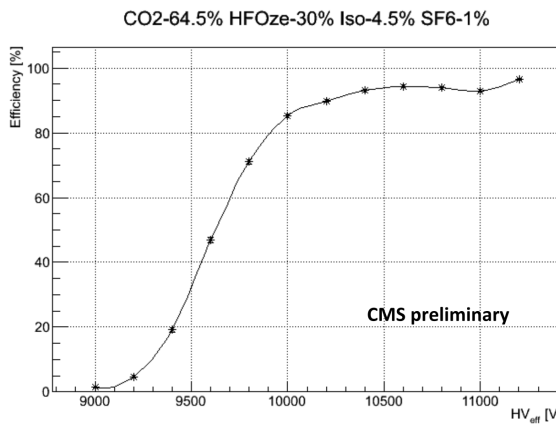


Figure 4.27: Efficiency of a CMS double-gap RPC operated with 30% of HFO , 4.5% of iC_4H_{10} , 1% of SF_6 and 64.5% of CO_2 [203].

Preliminary studies conducted in Ghent confirmed that CO_2 alone would require more than 1% of SF_6 to reach full efficiency, as presented in Figure 4.26. Even though the results obtained in Ghent don't show the streamer probability (the probability to have very large avalanches whose induced charge is greater than 20 pC), the variation of the cluster size indicates that the streamers become predominant before the efficiency plateau is reached. Then, a very first test with an HFO/CO_2 was performed. Only one ratio was tested as can be seen from Figure 4.27 that displays a good efficiency with a plateau located at a similar high voltage than with $R134a$ based mixtures (Figure 4.28). The status of RPC studies is presented in Figure 4.28 in which the performance (efficiency and streamer probability) of a CMS double-gap RPC operated with alternative gas mixtures is compared to the present CMS RPC mixture. Although the efficiency of detectors operated with mixtures containing CO_2/CF_3I or CO_2/HFO as a replacement for $C_2H_2F_4$ seems to reach similar levels than which of the detectors operated with the present mixture, the new gas mixtures feature a streamer probability that far exceeds which of the present fluorinated mixture. The SF_6 doesn't seem to prevent the formation of streamers as efficiently even when used at levels more than three times higher than with the standard CMS RPC mixture. Nevertheless, it is important to note that these results were obtained with a single-gap RPC while the use of a double-gap RPC reduces the operation voltage by 200 to 300 V, lowering the induced charge. A compromise in between good efficiency and acceptable level of streamer probability, and the fine-tuned composition of potential replacement gas mixtures will be kept on being studied using a standard double-gap CMS RPC.

Although the technology certification was conducted with the standard CMS gas mixture which is a known reference, the iRPCs will need to be operated with new environmental-friendly gas mixtures. Studies have then been conducted with iRPCs, assuming that the HFO/CO_2 mixture contain-

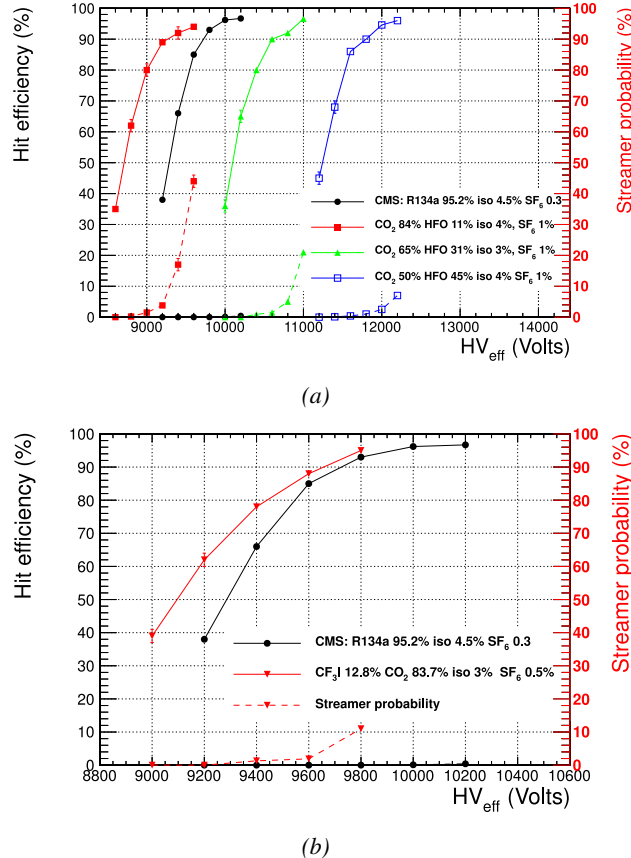


Figure 4.28: The efficiency (solid lines) and streamer probability (dashed lines) of HFO/CO_2 (a) and CF_3I/CO_2 (b) based gas mixtures as a function of the effective high-voltage are compared with the present CMS RPC gas mixture represented in black [177, 203]. The detector used for the study is a single-gap RPC with similar properties than CMS RPCs. The streamer probability is defined as the proportion of events with a deposited charge greater than 20 pC.

ing an almost equal level of both components was the most likely candidate to replace the standard mixture. In this purpose, an iRPC prototype has been built to be tested with an HFO/CO_2 gas mixture. The mixture, referred to as "ecogas" in Figure 4.29, contained 50% of HFO , 4.5% of iC_4H_{10} , 0.3% of SF_6 and 45.2% of CO_2 . In Figure 4.29 is presented a result consistent with the blue curve obtained with 45% of HFO , 4% of iC_4H_{10} , 1% of SF_6 and 50% of CO_2 flushed into a standard double-gap RPC. Instead of the streamer probability, the cluster size is shown. The average number of hits generated by a muon passing through the chamber seem to have increased by 1 at the level of the knee of the sigmoid plateau using the ecogas.

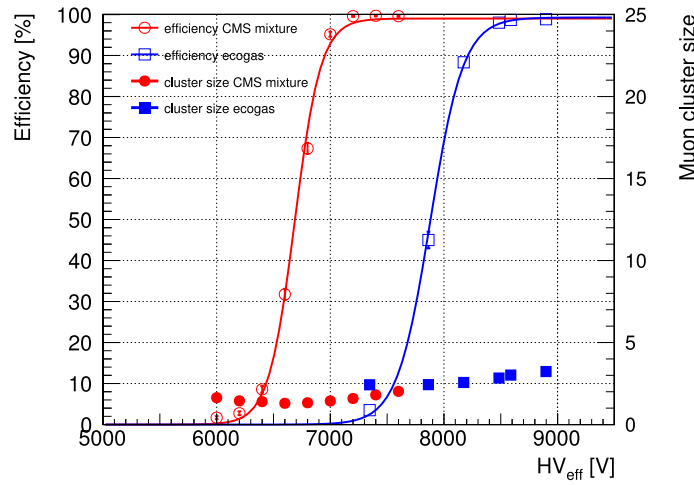


Figure 4.29: Efficiency (open symbols) and cluster size (full symbols) of an iRPC as a function of the effective voltage for the standard CMS gas mixture and an environmental-friendly gas mixture [177].